PCCP

PAPER

View Article Online
View Journal | View Issue

Cite this: *Phys. Chem. Chem. Phys.*, 2022, **24**, 23289

Physical and electrochemical properties of new structurally flexible imidazolium phosphate ionic liquids†

Sourav Bhowmick,* Andrei Filippov, Inayat Ali Khan and Faiz Ullah Shah*

New structurally flexible 1-methyl- and 1,2-dimethyl-imidazolium phosphate ionic liquids (ILs) bearing oligoethers have been synthesized and thoroughly characterized. These novel ILs revealed high thermal stabilities, low glass transitions, high conductivity and wide electrochemical stability windows up to 6 V. Both the cations and anions of 1-methyl-imidazolium ILs diffuse faster than the ions of 1,2-dimethyl-imidazolium ILs, as determined by pulsed field gradient nuclear magnetic resonance (PFG-NMR). The 1-methyl-imidazolium phosphate ILs showed relatively higher ionic conductivities and ion diffusivity as compared with the 1,2-dimethyl-imidazolium phosphate ILs. As expected, the diffusivity of all the ions increases with an increase in the temperature. The 1-methyl-imidazolium phosphate ILs formed hydrogen bonds with the phosphate anions, the strength of which is decreased with increasing temperature, as confirmed by variable temperature ^{1}H and ^{31}P NMR spectroscopy. One of the representative IL, **[EmDMIm][DEEP]**, presented promising elevated temperature performance as an electrolyte in a supercapacitor composed of multiwall carbon nanotubes and activated charcoal (MWCNT/AC) composite electrodes.

Received 3rd July 2022,
Accepted 8th September 2022

DOI: 10.1039/d2cp03022e

rsc.li/pccp

Introduction

Ionic liquids (ILs) have been extensively used as green solvents in organic synthesis,[1,2] as non-volatile thermally and electrochemically stable electrolytes in batteries,[3] fuel cells,[4] electrochemical sensors,[5] in homogeneous and heterogeneous catalysis,[6] and, more recently, in asymmetric organic synthesis.[7] The structural designability of both cations and anions in ILs make them suitable candidates for a variety of applications.[8] ILs are popular not only for their wide applicability range but also for their important physicochemical properties such as non-flammability, low vapor pressure, a vast liquidus range, excellent thermal stability, and wide electrochemical stability.[9,10] The permanent charges on ILs expand their potential applicability in new applications such as electroactive devices and actuators.[11] In such applications, ILs enhance the existing films upon swelling, which tends to enhance the conductivity of actuators.[12] In this context, research interest is growing to explore new versatile ILs in the preparation of novel ionic materials based on the remarkable capabilities of ILs.[13]

The ILs based on the imidazolium ring are very adaptable scaffolds that are becoming increasingly popular in a variety of applications including biphasic reaction catalysis,[14] electromechanical actuator membranes,[15] diluents,[16] separation research membranes,[17] and water purification agents, among others.[18] Imidazolium-based ILs were initially introduced in 1984, and since then, interest in their chemistry has exponentially accelerated.[19] When the tertiary nitrogen atom is quaternized, the imidazolium ring current is easily ionized, resulting in a permanently positively charged cation. Like other ILs, imidazolium-based ILs have a number of advantages including a constant charge,[20] the capacity to act as green solvents,[21] and high thermal stability.[22] Imidazolium-based ILs are also known for their potential as green organic solvents in different applications due to their non-volatility and structural desiganability.[23–25] The potential characteristics of imidazolium-based ILs can be tuned by functionalizing the ring with various alkyl substituents and combining the cation with different counter anions. Imidazolium-based ILs have also received growing attention for a variety of reasons including high thermal stability, relatively high ionic conductivity, a broad electrochemical window, amphoteric features and plastic crystalline behavior.[26–29]

As with all other ILs, the imidazolium cation can be coupled to a task-specific counter anion to boost the solubility, ionic conductivity and electrochemical properties as electrolytes in energy storage devices (ESDs).[30] Due to the growing interest in electrification, ESDs including batteries and supercapacitors (SCs) are the most widely utilized energy storage systems.[31,32]

Chemistry of Interfaces, Luleå University of Technology, SE-971 87 Luleå, Sweden. E-mail: sourav.bhowmick@associated.ltu.se, faiz.ullah@ltu.se

† Electronic supplementary information (ESI) available. See DOI: https://doi.org/10.1039/d2cp03022e

Compared to batteries, SCs have a high power output and a long cycle life, and can be used either alone or in combination with batteries in a variety of applications including electric buses, light rail, wearable electronics, and energy storage systems for intermittent renewable energy sources.[33,34] Independent of the type of ESD, an electrolyte plays a key role in their overall performance, service life and safety.

In this context, great interest is seen in phosphate-based electrolytes due to the safety considerations, optimizing separators[35] and electrode materials,[36] as well as overcharge shielding and redox-shuttle species.[37,38] The choice of an electrolyte lowers the safety risk of ESDs, especially when a non-flammable electrolyte is used.[39] The use of flame-retarding chemicals can improve the fire properties of electrolytes by reducing the flammability of the electrolytes.[40–44] Organophosphorus compounds,[45,46] fluorinated ethers[47] or esters,[48] fluorinated sulfones,[49] and ionic liquids[50,51] have all been studied to improve the fire properties of electrolytes. However, the disadvantage of using organophosphorus compounds as flame-retardants is their poor electrochemical compatibility with lithium battery electrodes.[52–54] Interestingly, ILs provide many unique properties in addition to non-flammability and improved electrochemical behavior, as discussed earlier.

In this study, we introduce new classes of ambient temperature liquid imidazolium-phosphate ILs with oligoether alkyl chains linked to both the cations and the anions. The design motif for developing these ILs is that the phosphorus moiety might improve the flame-retardant properties,[55] whereas the ethylene oxide units of the alkyl chains provide structural flexibility. Multinuclear (^{1}H, ^{13}C, and ^{31}P) nuclear magnetic resonance (NMR) spectroscopy and mass spectrometry analysis are used to analyze the purity and chemical structures of the products. Systematic physicochemical and electrochemical properties of all the ILs are evaluated and discussed in detail.

Results and discussion

The synthesis and structural characterizations of the ILs are described first, followed by a thorough investigation of the thermal behavior, ionic conductivity and ion diffusivity. Variable-temperature ^{1}H and ^{31}P NMR spectroscopy is used to investigate the interactions between the imidazolium cations and the phosphate anions in the neat ILs. Finally, the electrochemical stability of all the neat ILs and the electrochemical performance of one representative IL as an electrolyte in a supercapacitor is discussed.

Synthesis and characterization

The imidazolium-based ILs have been synthesized *via* a single step reaction using trialkyl phosphate with longer oligoether-based chains (Scheme 1) as a synthon. Trialkyl phosphate reacts with the respective 1-methyl-imidazole and 1,2-dimethyl-imidazole without any solvent in a 1 : 1 stoichiometric ratio at 80 °C for four days to obtain the corresponding **[MmMIm][TEEP]** and **[MmDMIm][TEEP]** ILs in a single step with high yield (Scheme 1).

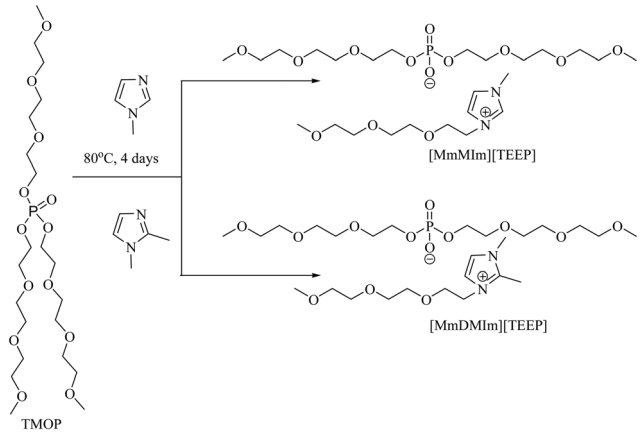

Scheme 1 Synthesis of **[MmMIm][TEEP]** and **[MmDMIm][TEEP]** ionic liquids.

Using the same protocol shorter oligoether-based chain ILs are synthesized by reacting trialkyl phosphate with either 1-methyl-imidazole or 1,2-dimethyl-imidazole in a 1 : 1 stoichiometric ratio to obtain **[EmMIm][DEEP]** and **[EmDMIm][DEEP]** ILs with high yield (Scheme 2).

The new ILs are characterized by multinuclear (^{1}H, ^{31}P and ^{13}C) NMR spectroscopy and mass spectrometry analysis. The ^{31}P{^{1}H} NMR spectra of these ILs reveal single and symmetric resonance lines, confirming completion of the reaction between the trialkyl phosphate and the corresponding imidazole. The ^{31}P resonance lines are shifted by $\Delta\delta$ = 1.63 and 1.04 ppm for ILs **[MmMIm][TEEP]** and **[MmDMIm][TEEP]**, respectively, as compared with the neutral trialkyl phosphate synthon. A similar shift is observed for the other two ILs as well. The ^{1}H NMR spectra of these ILs also confirmed the formation and purity of the synthesized ILs. In the ^{1}H NMR spectrum of **[MmMIm][TEEP]** IL, three singlet resonance lines appeared at 10.43, 7.58 and 7.28 ppm, and are assigned to the protons of the imidazolium unit. The ^{1}H resonance lines at 4.54–4.52, 3.99–3.95, 3.83–3.81, 3.64–3.57, 3.50–3.49 and 3.33 ppm are attributed to the ether moieties of the anion and the cation in

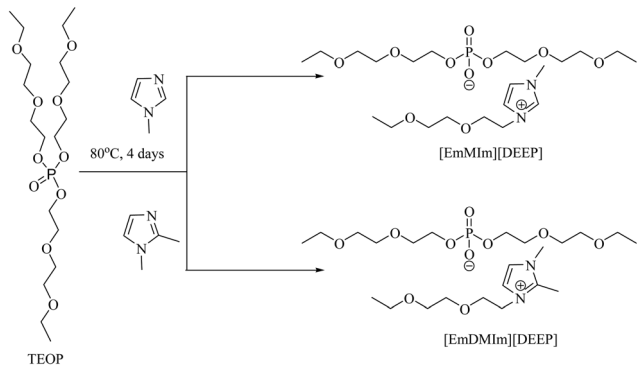

Scheme 2 Synthesis of **[EmMIm][DEEP]** and **[EmDMIm][DEEP]** ionic liquids.

[MmMIm][TEEP] IL. Similarly, all ^{1}H resonance lines are assigned in the case of the other three ILs. In addition, the $^{13}C\{^{1}H\}$ NMR spectra showed all the characteristic resonance lines for both the cation and anion in these ILs. All the NMR spectra are provided in the ESI.†

Thermal properties

TGA thermograms of the imidazolium-phosphate ILs are shown in Fig. 1(a). The decomposition temperatures (T_d), as determined from the intersection of the baseline weight and the tangent of the weight dependency on the temperature curve, have been used to characterize the thermal stability of the ILs. The $[TEEP]^-$ anion based ILs show up to 10 °C higher decomposition temperatures than the ILs with the $[DEEP]^-$ anion. The extra methyl group attached to the imidazolium ring has revealed no significant influence on the thermal stability of these ILs. The T_d of these four functionalized imidazolium-phosphate ILs occur within a narrow temperature range from 252 to 260 °C (Table 1). Overall, the thermal stability of these ILs is comparable and/or better than the reported ILs with imidazolium cations.[56–58]

The DSC curves are shown in Fig. 1(b) and the values of glass transition temperatures (T_g) are tabulated in Table 1. The DSC data demonstrated that all these ILs are glass forming liquids, as suggested by the T_g in the temperature range from −70 to −75 °C (Fig. 1(b)). When compared to the 1,2-dimethylimidazolium-based ILs, the 1-methylimidazolium-based ILs revealed slightly lower T_g values. In addition, the ILs with $[TEEP]^-$ anions showed relatively higher T_g values as compared to the ILs with $[DEEP]^-$ anions. The main differences in these two ILs are the lengths of the oligoether chains attached to both the anions and the cations, and the terminal alkoxide units. This DSC data indicate that the presence of terminal ethylene oxide units play a key role in lowering the glass transition temperature by permitting low-energy rotations of the two alkyl chains.[59]

In general, the ILs exhibiting a freezing transition when cooled have a high proclivity for producing crystals. In this context, crystal packing is an intriguing phenomenon that is dependent on many non-covalent intra and inter molecular interactions including as ion–ion, ion–dipole, dipole–dipole,

Table 1 Molecular weights, glass transition temperatures, decomposition temperatures, and ionic conductivity of the imidazolium-phosphate ionic liquids

Ionic liquid	M_w (g mol^{-1})	T_d (°C)	T_g (°C)	σ (mS cm^{-1}) at 25 °C	σ (mS cm^{-1}) at 100 °C
[MmMIm][TEEP]	618.65	260	−70	0.1	1.9
[EmMIm][DEEP]	528.57	250	−74	0.08	1.8
[MmDMIm][TEEP]	632.68	258	−72	0.07	1.4
[EmDMIm][DEEP]	542.60	252	−75	0.05	1.3

hydrogen bonding, van der Waals forces, *etc.*[60–62] In the case of our ILs, the key determinant of crystal packing is the ion–ion interactions between the imidazolium cations and the phosphate-based anions. In this case, the stronger ion–ion interactions cause crystal packing in the structures and affect the T_g values. The T_g values are also affected by the nature of alkyl chains. It is known that T_g values decrease when ether groups are incorporated into the alkyl side chain of the ion.[63] We observed that the ILs with larger number of ethylene oxide units in the alkyl chains have slightly higher glass transition temperatures than the ILs with a fewer number of ethylene oxide units. This increase in the glass transition temperatures might be due to the enhanced polarity with increasing ethylene oxide units in the alkyl chains, facilitating efficient crystal packing of the ions.

Ionic conductivity

Ionic conductivity is one of the most essential characteristics of ionic materials, particularly when used as electrolytes in energy storage devices. Ionic conductivity of the imidazolium-phosphate ILs is measured over a wide temperature range from −20 to 100 °C (Fig. 2). As expected, a sharp increase in the ionic conductivity of all the ILs is observed with increasing temperature, which is due to the decrease in the ionic interactions leading to ion dissociation at elevated temperatures. The ILs with longer oligoether chains showed higher ionic conductivity than the ILs with shorter oligoether chains. The ionic conductivity of **[MmMIm][TEEP]** and **[EmMIm][DEEP]** ILs is higher throughout the whole studied temperature range as compared with the methyl substituted imidazolium-phosphate ILs,

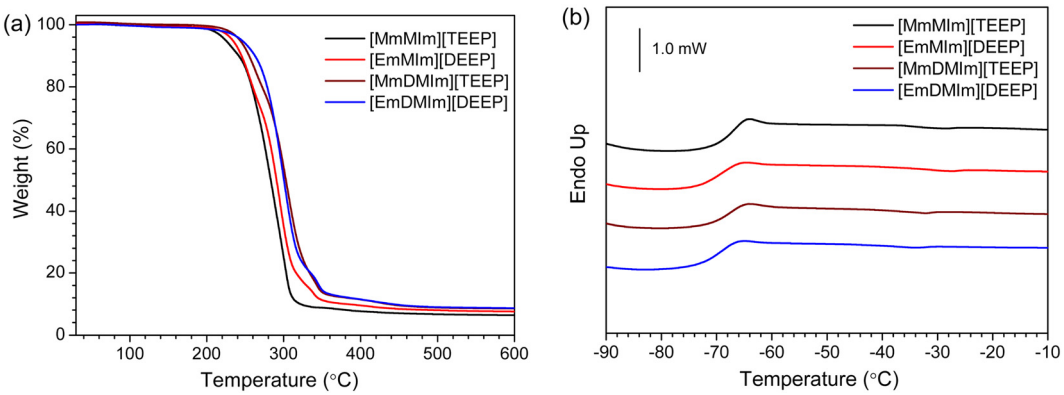

Fig. 1 (a) TGA thermograms and (b) DSC curves of the imidazolium-phosphate ionic liquids.

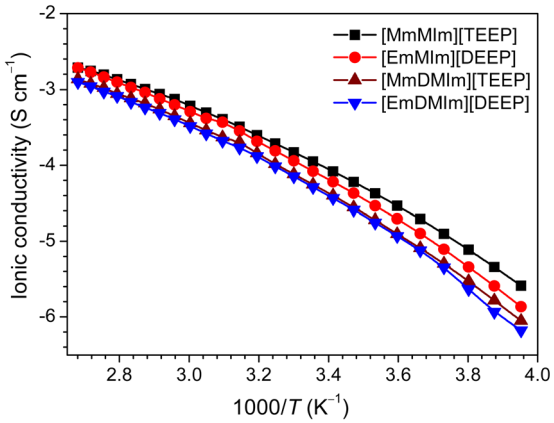

Fig. 2 Ionic conductivity of the imidazolium-phosphate ionic liquids. The symbols indicate experimental points and the lines represent the best fits to the VFT equation.

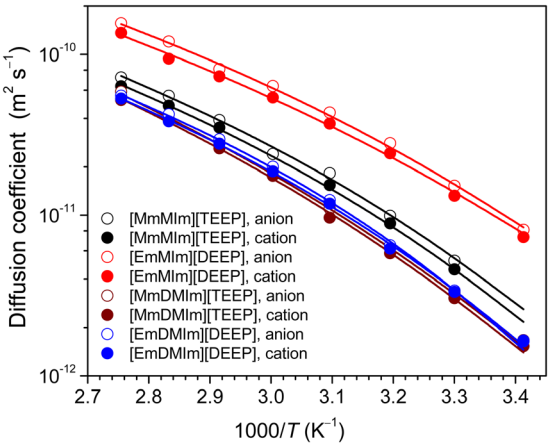

Fig. 3 Diffusion coefficients of ions in imidazolium–phosphate ionic liquids. The symbols represent experimental points and the lines are best fits to the VFT equation.

[MmDIm][TEEP] and **[EmDMIm][DEEP]**. Despite their similar chemical structures, the latter contain extra methyl groups attached to the imidazolium ring of the cation and increased cation size resulting in lower ionic conductivity. It is also found that the ionic conductivity increases with an increase in the number of ethylene oxide units of the alkyl chains of cation and anions.

The ionic conductivity data is fitted to the Vogel–Fulcher–Tammann (VFT) eqn (1). Nonlinear fits are used to obtain the VFT parameters (Table S2, ESI†).

$$\sigma = \sigma_0 \exp\left(\frac{-B}{(T - T_0)}\right) \quad (1)$$

where σ_0 is a pre-exponential factor, B a factor related to the activation energy and T_0 is the ideal glass transition temperature. The energy of activation for ionic conductivity is related to B as $E_\sigma = B{\cdot}R$. The T_g values obtained from the DSC data are larger for these ILs than the reference T_0 values. The $T_g - T_0$ values are about 50 K, which is in accordance with the empirical approximation for ionic liquids.[64] The E_σ are comparable for these ILs.

NMR diffusometry

PFG NMR diffusometry is employed to better understand the relative ionic mobility in the imidazolium-phosphate ILs as a function of temperature (Fig. 3). It is clear that diffusivity of all the ions increases with increasing temperature as a result of thermal activation of the diffusion process. Both the cation and anion in **[EmMIm][DEEP]** IL diffuse much faster than the ions in **[MmMIm][TEEP]** IL, which is obvious because the latter IL has relative larger sizes and masses of both anion and cation. Similarly, the same is true for the faster ion diffusion in **[EmDMIm][DEEP]** IL than in **[MmDMIm][TEEP]** IL. The extra methyl group attached to the imidazolium ring increases mass of the cation resulting in a comparatively slower diffusion of ions in **[MmDMIm][TEEP]** and **[EmDMIm][DEEP]** ILs. Another plausible explanation is the positive inductive effect of the methyl group in the 1,2-dimethyl-imidazolium ring, stabilizing the positive charge on the nitrogen centre. The **[MmDMIm][TEEP]** and **[EmDMIm][DEEP]** ILs are stabilized by the positive inductive effect, leading to stronger interactions between the cations and the anions, and thus a slower ion mobility.

The diffusivity is further analyzed by fitting the data into the VFT equation over a wide temperature range. The following Arrhenius equation describes the temperature dependency:

$$D(T) = D_0 \cdot \exp\left(\frac{-E_D}{RT}\right) \quad (2)$$

where D_0 denotes a temperature-independent parameter, E_D is the molar activation energy of diffusion and R is the gas constant. In Arrhenius coordinates, the Arrhenius function has a linear dependence $D(T)$, which is not the case for these ILs. For many ILs, non-Arrhenius dependences are common.[65,66] The reason for this is that the glass transition temperature, T_0, is close to the measurement temperature. Under such conditions, the diffusion data are better analyzed using a VFT equation (eqn (3)).

$$D = D_0 \exp\left(\frac{-B}{(T - T_0)}\right) \quad (3)$$

where T_0 and B are variables that can be changed. As $E_D = B{\cdot}R$, the activation energy for diffusion is related to B. In the high-temperature range ($T_0 \rightarrow 0$), this form is equivalent to the Arrhenius dependency. The corresponding fitting parameters are tabulated in Table S3 (ESI†). The ions in **[EmMIm][DEEP]** IL have much larger D_0 values (more than twice) than the ions in **[MmMIm][TEEP]** IL. The values of D_0, on the other hand, are opposite for **[MmDMIm][TEEP]** and **[EmDMIm][DEEP]** ILs. The ions in **[MmDMIm][TEEP]** IL have significantly higher D_0 values (more than twice) than the ions in **[EmDMIm][DEEP]**.

^{1}H and ^{31}P NMR spectroscopy

Variable temperature ^{1}H and ^{31}P NMR spectroscopy is employed in order to better understand the changes in the local environment of the ions as a function of temperature.

An instant observation of Fig. 4 is that the chemical environment of phosphorus atom in the phosphate anions is temperature dependent. A substantial downfield shift is observed in the ^{31}P NMR resonance lines of all the four ILs with an increase in the temperature, clearly reflecting on the decrease in ionic interactions between the phosphate anions and the imidazolium cations. The lower ionic interactions further lead to a decrease in the electron shielding effect from the phosphorus nucleus in the phosphate anions, and thus facilitating the phosphorus atom of the cation to become more positively charged leading to a downfield chemical shift.

A clear evidence of hydrogen bonding between the imidazolium cations and the phosphate anions is seen by analyzing the variable temperature ^{1}H NMR spectra of these ILs (Fig. 5). The appearance of broad ^{1}H resonance lines in the case of neat ILs, in comparison to the resonance lines of the same samples dissolved in $CDCl_3$, is due to the incomplete averaging of the dipole–dipole spin interactions in these viscous systems. A significant downfield change in the ^{1}H NMR chemical shift of N–CH═N– group present in the imidazolium ring of **[MmMIm][TEEP]** and **[EmMIm][DEEP]** ILs is seen with increasing temperature (Fig. 5(a) and (b)). This shift points towards hydrogen bonding between the proton of N–CH═N– group and oxygen atoms present in the phosphate anion, the strength of which decreases by increasing the temperature leading to cation–anion dissociation. Electron density of the hydrogen-bonded proton gradually decreases with an increase with temperature resulting in a downfield shift in the ^{1}H NMR resonance line. The hydrogen bonding is further confirmed by the shift in ^{1}H NMR resonance lines for the protons in close vicinity of the oxygen atoms in the phosphate anion (Fig. S23 in the ESI†). Here it is noteworthy that the ^{1}H NMR resonance lines of the –CH═CH– group in the 1,2-dimethyl-imidazolium ring are less affected with an increase in temperature, indicating that these protons are less influenced by the hydrogen bonding (Fig. 5(c) and (d)). It is already known that the proton in the N–CH═N– group of the imidazolium cation is acidic and can spontaneously be released leading to formation of the N-heterocyclic carbene.[67] However, there is no evidence of spontaneous carbene formation in these ILs.

Electrochemical stability

It is critically important to investigate the electrochemical stability of an electrolyte before using it in an electrochemical energy storage device. Fig. 6 shows the cathodic and anodic scans of the LSV curves for the neat imidazolium-phosphate ILs on the platinum working electrode at 20 °C and the values of respective cathodic (E_c) and anodic (E_a) limits are tabulated in Table S1 (ESI†). Overall, the 1,2-dimethylimidazolium-based ILs have revealed much wider ESWs

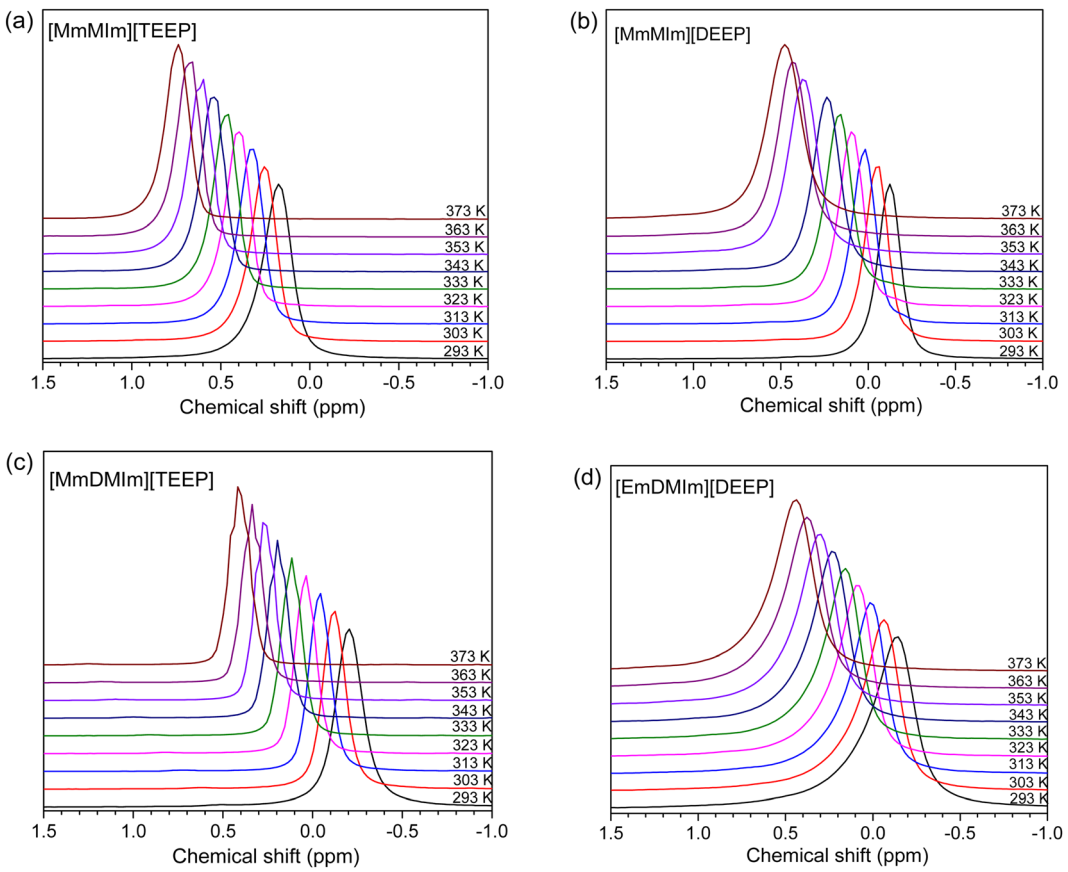

Fig. 4 ^{31}P NMR spectra of the neat imidazolium-phosphate ionic liquids (a–d) as a function of temperature.

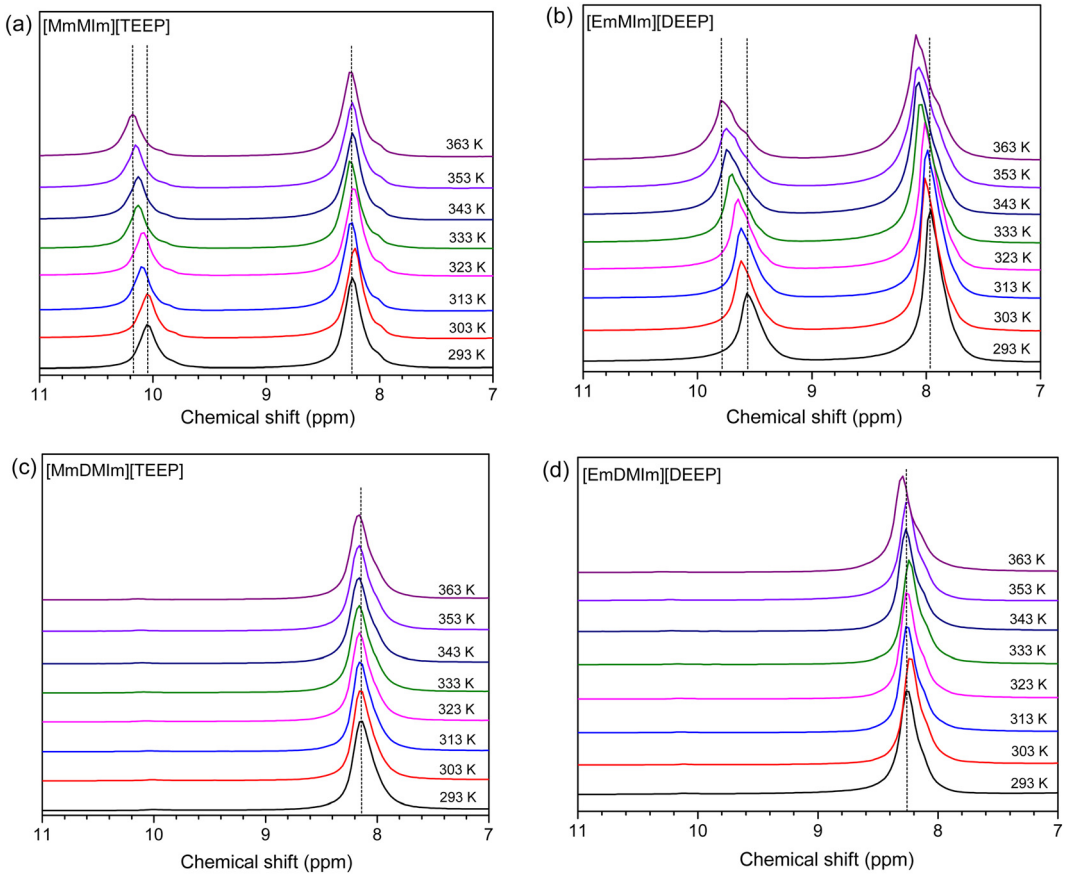

Fig. 5 ^{1}H NMR spectra of the neat imidazolium-phosphate ionic liquids (a–d) as a function of temperature.

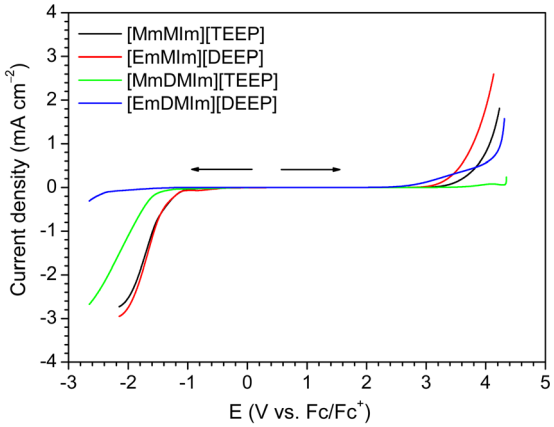

Fig. 6 Cathodic and anodic LSV curves of the neat imidazolium-phosphate ionic liquids on the Pt working electrode at 20 °C temperature.

than the 1-methylimidazolium-based ILs. For both **[MmMIm][TEEP]** and **[MmDMIm][TEEP]**, the ESWs are getting wider as the oligoether chain length increases at the imidazolium cation and at the phosphate anion suggesting that the increasing number of ethylene oxide units in the chains contribute to the electrochemical stability. Among these four different ILs, **[MmDMIm][TEEP]** provide the largest ESW due to the combination of the 1,2-dimethylimidazolium-based cation and the longer oligoether chains in both the cation and the anion.

The different scan rates CVs at 20 °C of the supercapacitor is presented in Fig. 7. The shape of voltammograms gradually changes from less distorted to a completely elongated shape with increasing scan rate from 0.002 to 0.100 V s^{-1} revealing an acceptable capacitive behavior (Fig. 7(a)). The distorted pattern of the CV curves with scan rates indicates that the **[EmDMIm][DEEP]** IL is not suitable for quick charge and discharge conditions at ambient temperature. The supercapacitor reveals lower current and specific capacitance at lower scan rates but increases with an increase in the scan rates. This inverse relation of capacitance *versus* scan rate can be explain by the ion interactions with the electrode materials. At lower scan rates, the ions have enough time to interact and accommodate in the smaller pores of the electrodes producing higher current and capacitance. However, at a higher sweep rates the ions can interact and accommodate only in the larger pores and, therefore, produced a lower capacitance.[68–70] An inverse relation of capacitance retention as a function of potential scan rates is shown in Fig. 7(b). The capacitor retained about 41.7%, 33.3% and 20.8% of its initial capacitance at 0.020, 0.050 and 0.100 V s^{-1}, respectively.

The shape of CV curves get more rectangular with an increase in the temperature (Fig. 8(a)) and the current and

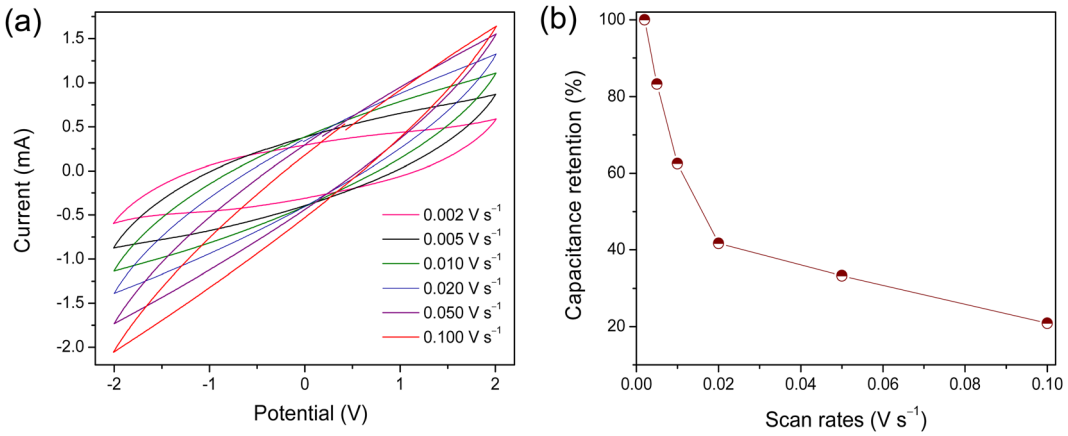

Fig. 7 CV curves (a) and capacitance retention (b) as a function of potential scan rates for the supercapacitor composed of MWCNTs/AC composite electrodes and **[EmDMIm][DEEP]** IL as an electrolyte.

the specific capacitance increase continuously with increasing temperature. A steady increase in the capacitance retention with an increase in the temperature is also found (Fig. 8(b)). This increase in the specific capacitance with an increase in the temperature can be described by the higher ionic mobility of the IL electrolyte at elevated temperature, resulting in a higher ionic conductivity and ion–surface interactions. The relatively higher specific capacitance at higher temperatures (40 F g^{-1} at 100 °C, at 0.005 V s^{-1}) can also be explained from the variable temperature impedance spectra of **[EmDMIm][DEEP]**-MWCNTs/AC composite supercapacitor as shown in Fig. S26 (ESI†), where the solution resistance and charge transfer resistance are greatly reduced at high temperatures.

Conclusions

The newly synthesized oligoether functionalized imidazolium-phosphate ILs revealed excellent thermal and electrochemical stabilities, low glass transition temperatures, and promising ionic conductivity. The ILs with smaller ion sizes showed lower ionic conductivity but faster ion diffusivity, and *vice versa*. The ions diffused much faster in the case of 1-methyl-imidazolium based ILs than in the 1,2-dimethyl-imidazolium based ILs. As expected, an increase in the ionic conductivity and ion diffusivity is observed with an increase in the temperature due to the ion dissociation at elevated temperatures. A temperature dependent hydrogen bonding is observed in the case of 1-methyl-imidazolium based ILs, as revealed by variable temperature ^{1}H and ^{31}P NMR spectroscopy. Overall, these new classes of ILs exhibit promising physicochemical and electrochemical properties over a wide temperature range. This study provides a foundation to the development of fluorine-free and structurally flexible ionic liquid-based electrolytes for next generation energy storage devices.

Experimental

Materials

TMOP and TEOP have been synthesized using phosphorus(v) oxychloride (99% purity, Sigma Aldrich) and respective alcohol triethylene glycol monomethyl ether (95% purity, Sigma Aldrich) and di(ethylene glycol) ethyl ether (99% purity, Sigma

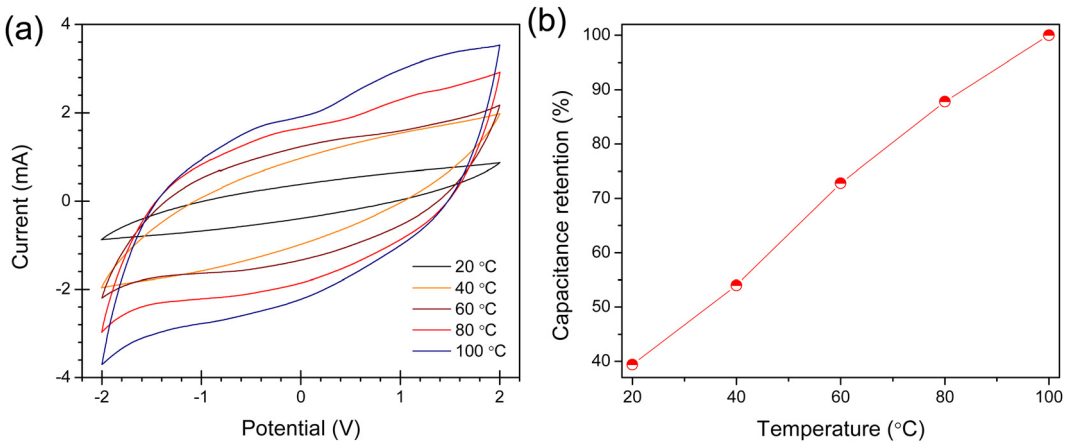

Fig. 8 CV curves (a) and capacitance retention (b) as a function of temperature for the MWCNTs/AC composite electrodes and **[EmDMIm][DEEP]** IL electrolyte supercapacitor.

Aldrich). 1-Methylpyrrolidine (98% purity, Sigma Aldrich) 1,2-dimethylimidazole (99% purity, Sigma Aldrich), 1-methylimidazole (98% purity, Sigma Aldrich), sodium sulfate (99% purity, Sigma Aldrich), ethyl acetate (99.5% purity, Sigma Aldrich) and hexane (99% purity, Sigma Aldrich) were used without further purification. All the synthesized ILs were kept in a vacuum oven at 90 °C for at least 3 days until the water content was less than 100 ppm (Table S4, ESI†), as determined by the Karl–Fischer titration using a 917 coulometer (Metrohm) placed inside a glovebox with water and oxygen contents less than 1 ppm. Multi-walled carbon nanotubes (Sigma Aldrich, 95% carbon, O.D. × L 6–9 nm × 5 μm), activated charcoal (Sigma Aldrich, 100 mesh size), polyvinyl alcohol (Merck, M_W 72 000) and glass microfiber filters (Whatman®) were used as received.

Synthesis of [MmMIm][TEEP]and [MmDMIm][TEEP]

Triphosphate ester TMOP (10.00 g, 18.64 mmol) and 1-methyl-1*H*-imidazole (1.49 ml, 18.64 mmol) were taken in a Schlenk flask in an inert atmosphere. The reaction mixture was heated at 80 °C in an inert atmosphere for 4 days. After completion, the reaction mixture was washed with hexane three times to get the desired IL. The remaining solvent was evaporated using a rotary evaporator and the IL was placed in a vacuum oven at 90 °C for at least 3 days.

[MmMIm][TEEP]. Yield: 11.10 g, 96%. ^{1}H NMR (400 MHz, $CDCl_3$): δ 3.33 (s, 9H), 3.64–3.49 (m, 29H), 3.83–3.81 (m, 2H), 3.99–3.95 (m, 6H), 4.54–4.52 (m, 2H), 7.26 (s, 1H), 7.58 (s, 1H), 10.43 (s, 1H). ^{31}P{^{1}H} NMR (162 MHz, $CDCl_3$): δ 0.60. ^{13}C NMR ($CDCl_3$, 100 MHz): δ 139.46, 123.48, 122.46, 72.05, 72.00, 71.36, 71.28, 70.74, 70.53, 70.48, 70.45, 70.38, 70.30, 69.44, 64.31, 64.25, 59.03, 49.64, 36.41. IR (ATR): 2878.06, 1569.67, 1456.45, 1355.81, 1255.16, 1104.19, 1066.45, 953.22, 852.58, 789.67, 656.79, 627.44 cm^{-1}. MS (ESI). $[C_{11}H_{21}N_2O_3]^+$: calcd for *m*/*z* 229.15. Found *m*/*z* 229.157, MS (ESI). $[C_{14}H_{30}O_{10}P]^-$: calcd for *m*/*z* 389.16. Found *m*/*z* 389.162.

[MmDMIm][TEEP]. Yield: 11.45 g, 97%. ^{1}H NMR (400 MHz, $CDCl_3$): δ 2.68 (s, 3H), 3.31 (s, 9H), 3.61–3.41 (m, 29H), 3.81–3.79 (m, 2H), 3.92–3.88 (m, 6H), 4.47–4.44 (m, 2H), 7.61–7.60 (d, J = 1.6 Hz, 1H), 7.78–7.77 (d, J = 1.6 Hz, 1H). ^{31}P{^{1}H} NMR (162 MHz, CDCl3): δ 0.01. ^{13}C NMR ($CDCl_3$, 100 MHz): δ 144.86, 122.94, 122.25, 72.03, 71.98, 71.41, 71.33, 70.73, 70.49, 70.43, 70.40, 69.68, 64.14, 64.09, 59.03, 59.01, 48.94, 35.53, 10.33. IR (ATR): 2878.06, 1599.67, 1536.77, 1461.29, 1360.64, 1247.41, 1209.67, 1096.45, 1071.29, 945.48, 857.41, 781.93, 668.70 cm^{-1}. MS (ESI). $[C_{12}H_{23}N_2O_3]^+$: calcd for *m*/*z* 243.17. Found *m*/*z* 243.171, MS (ESI). $[C_{14}H_{30}O_{10}P]^-$: calcd for *m*/*z* 389.16. Found *m*/*z* 389.159.

Synthesis of [EmMIm][DEEP] and [EmDMIm][DEEP]

Triphosphate ester TEOP (10.00 g, 22.39 mmol) and 1-methyl-1*H*-imidazole (1.78 ml, 22.39 mmol) were taken in a Schlenk flask in an inert atmosphere. The reaction mixture was heated at 80 °C in an inert atmosphere for 4 days. After completion, the reaction mixture was washed with hexane three times. The solvent was evaporated in a rotary evaporator and the product was placed in vacuum oven at 90 °C for at least 3 days.

[EmMIm][DEEP]. Yield: 11.4 g, 96%. ^{1}H NMR (400 MHz, $CDCl_3$): δ 1.15–1.13 (t, 9H), 3.63–3.45 (m, 22H), 3.82 (s, 2H), 3.99 (s, 6H), 4.53 (s, 2H), 7.32 (s, 1H), 7.55 (s, 1H), 10.45 (s, 1H). ^{31}P{^{1}H} NMR (162 MHz, $CDCl_3$): δ 0.50. ^{13}C NMR ($CDCl_3$, 100 MHz): δ 139.33, 123.33, 122.58, 71.35, 71.27, 70.54, 69.97, 69.59, 69.40, 66.65, 66.60, 64.33, 64.28, 49.67, 36.49, 15.27. IR (ATR): 2865.48, 1582.25, 1456.45, 1355.80, 1247.41, 1110.12, 1072.25, 946.45, 782.90, 662.90, 625.16 cm^{-1}. MS (ESI). $[C_{10}H_{19}N_2O_2]^+$: calcd for *m*/*z* 199.14. Found *m*/*z* 199.146, MS (ESI). $[C_{12}H_{26}O_8P]^-$: calcd for *m*/*z* 329.14. Found *m*/*z* 329.139.

[EmDMIm][DEEP]. Yield: 11.60 g, 95%. ^{1}H NMR (400 MHz, $CDCl_3$): δ 1.21–1.18 (m, 9H), 2.73 (s, 3H), 3.57–3.45 (m, 14H), 3.67–3.63 (m, 8H), 3.87–3.85 (m, 2H), 3.91 (s, 3H), 3.99–3.96 (m, 4H), 4.51–4.49 (m, 2H), 7.58–7.56 (d, J = 1.6 Hz, 1H), 7.79–7.78 (d, J = 2.0 Hz, 1H). ^{31}P{^{1}H} NMR (162 MHz, $CDCl_3$): δ −0.03. ^{13}C NMR ($CDCl_3$, 100 MHz): δ 144.85, 122.90, 122.26, 71.41, 71.33, 70.66, 70.51, 70.01, 69.67, 69.64, 66.62, 64.25, 64.19, 49.04, 35.69, 15.30, 10.55. IR (ATR): 2865.48, 1599.67, 1549.35, 1461.29, 1360.64, 1247.41, 1109.03, 1071.29, 945.48, 781.93, 668.70 cm^{-1}. MS (ESI). $[C_{11}H_{21}N_2O_2]^+$: calcd for *m*/*z* 213.1 6. Found *m*/*z* 213.161, MS (ESI). $[C_{12}H_{26}O_8P]^-$: calcd for *m*/*z* 329.14. Found *m*/*z* 329.131.

NMR spectroscopy

The structure and purity of the newly synthesized ILs were characterized by using a Bruker Ascend Aeon WB 400 (Bruker BioSpin AG, Fällanden, Switzerland) nuclear magnetic resonance (NMR) spectrometer. $CDCl_3$ was used as a solvent for all these samples. The working frequencies were 400.21 MHz for ^{1}H, 100.64 MHz for ^{13}C and 162.01 MHz for ^{31}P. The ^{1}H and ^{31}P spectra of the neat ILs were recorded by placing the samples in a 5 mm standard NMR tube. The ^{1}H spectra were referenced to water (4.7 ppm) and ^{31}P spectra were referenced to phosphoric acid (0 ppm). Data were processed using Bruker Topspin 3.5 software.

Thermal analysis

A PerkinElmer 8000 TGA instrument was used for the thermogravimetric analysis (TGA). The temperature range was 303–873 K at 10 K min^{-1} under nitrogen as the inert atmosphere. The Pyris software was used to analyse the onset of decomposition temperature, T_{onset}, by taking the intersection of the baseline representing the weight loss and the tangent of the weight *vs.* temperature curve.[71]

Electrochemical measurements

The electrochemical measurements were carried out on an Autolab PGSTAT302N electrochemical workstation (FRA32 M module). The ionic conductivity was measured with a TSC 70 closed cell which is sealed with a Microcell HC cell stand, also connected to a temperature controller (RHD instruments, Germany). In the Microcell HC system, the temperature is measured through a Peltier element, which allows regulating the temperature from −20 to 100 °C. A two-electrode cell with Pt

wire as the working and Pt cup as the counter electrode was used for ionic conductivity measurements. The measurements were performed in the frequency range from 0.1 Hz to 1 MHz with an AC voltage amplitude of 10 mV_{rms}. The cell constant was determined by using a 100 μS cm^{-1} KCl standard solution from Metrohm (K_{cell} = 18.5396 cm^{-1}). The cell was thermally equilibrated for at least 10 min before each measurement.

The linear sweep voltammetry (LSV) was carried out at 20 °C temperature, using a standard three-electrode cell: Pt wire as a working electrode, a Pt cup as a counter electrode, and Ag wire (coated with AgCl) as a reference electrode. The LSV scan rate was 1 mV s^{-1} and electrochemical potentials were obtained with ferrocene as an internal reference. The ESW limits were determined using a 0.1 mA cm^{-2} cut-off current density. The electrodes were polished with a Kemet diamond paste 0.25 μm prior to each experiment.

The capacitive performance of **[EmDMIm][DEEP]** IL as an electrolyte is evaluated in a symmetrical two electrodes system at different scan rates of potential and variable temperatures using TSC battery cell (RHD instruments, Germany). The cell consists of stainless steel current collectors with an average contact area of 8 mm in diameter each. The electrode–separator–electrode sandwich assembly was adjusted between the cathode and the anode of the cell. The cell was crammed with screw cap and the contact pressure was adjusted with a gold platted spring having spring constant of 2.3 N mm^{-1} (40.7 kPa). The cell was assembled within a glovebox filled with nitrogen gas and water/oxygen levels less than 0.5 ppm.

The electrode material was prepared by stirrer-dispersing MWCNTs (60 wt%), activated charcoal (30 wt%) and polyvinyl alcohol (10 wt%, PVA) binder in distilled water for 24 h. After filtration and drying, the composite was finely ground and about 22 mg was pelletized at 80 MPa in a diameter of 10 mm. The supercapacitor was prepared by sandwiching the separator, 12 mm diameter glass microfiber filter-Whatman® previously soaked in the IL electrolyte, between the pellets. In the electrochemical tests, the capacitor was activated by recording an impedance spectra (from 1 MHz to 0.1 Hz at 10 mV amplitude) followed by 60 cycles of cyclic voltammetry at 0.005 V s^{-1} and at 20 °C (Fig. S24 and S25, ESI†). After the CV cycles, impedance was recorded again to check the cell resistance, and a decrease in the charge transfer resistance (R_{ct}) was found. Afterward, CVs were recorded at different scan rates (0.002–0.100 V s^{-1}) and at different temperatures (20–100 °C), interrupted by impedance measurements at each temperature. From CV tests, the specific capacitance (C_{sp}) was calculated by using eqn (4).[72]

$$C_{sp} = \frac{2I}{m\left(\frac{dv}{dt}\right)} \quad (4)$$

where I is the current (A), m is the mass loading of the electrode material (g), dv/dt is the potential scan rate (V s^{-1}).

NMR diffusometry

Pulsed gradient spin echo-nuclear magnetic resonance (PGSE-NMR) measurements were performed on a Bruker Ascend Aeon WB 400 (Bruker BioSpin AG,) NMR spectrometer. NMR self-diffusion measurements were performed on ^1H (400.21 MHz) using a PGSE-NMR probe Diff50 (Bruker). The sample was placed in a standard 5 mm glass sample tube and closed with a plastic stopper to avoid air contact. Prior to measurements, the sample were equilibrated at a specific temperature for 30 min. The diffusional decays (DD) were recorded using the stimulated echo (StE) pulse train. For single-component diffusion, the form of the DD can be described as[73]

$$A(\tau, \tau_1, g, \delta) \propto \exp\left(-\frac{2\tau}{T_2} - \frac{\tau_1}{T_1}\right) \exp\left(-\gamma^2\delta^2 g^2 D t_d\right) \quad (5)$$

Here, A is the integral intensity of the NMR signal, τ is the time interval between first and second radiofrequency pulses, τ_1 is the time interval between second and third radiofrequency pulses. γ is the gyromagnetic ratio for the magnetic nucleus (^1H); g and δ are the amplitude and the duration of the gradient pulse; $t_d = (\Delta - \delta/3)$ is the diffusion time; Δ is the time interval between two identical gradient pulses. D is the diffusion coefficient. In the measurements, the duration of the 90° pulse was 7 μs, δ was in the range of (0.5–2) ms, τ was in the range of (3–5) ms, and g was varied from 0.06 up to the maximum of the gradient amplitude, 29.73 T m^{-1}. Diffusion time t_d was varied from 4 to 100 ms and the repetition time during accumulation of signal transients was 3.5 s. Measurements were performed in the temperature range from 295 K to 373 K.

Author contributions

Sourav Bhowmick: synthesis, characterization, writing original draft. Andrei Filippov: NMR diffusometry, conceptualization, editing. Inayat Ali Khan: electrochemical measurements, editing. Faiz Ullah Shah: supervision, conceptualization, methodology, editing.

Conflicts of interest

There are no conflicts to declare.

Acknowledgements

The Kempe Foundation in memory of J. C. and Seth M. Kempe is gratefully acknowledged for the financial support in the form of a stipend for S. B. (grant numbers: SMK-1945 and SMK21-0013). The financial support from the Swedish Research Council (project number: 2018-04133) is gratefully acknowledged.

References

1 T. Welton, Room-temperature ionic liquids. solvents for synthesis and catalysis, *Chem. Rev.*, 1999, **99**, 2071–2084.
2 R. D. Rogers and K. R. Seddon, Ionic liquids–solvents of the future?, *Science*, 2003, **302**, 792–793.

3 Q. Li, J. Chen, L. Fan, X. Kong and Y. Lu, Progress in electrolytes for rechargeable Li-based batteries and beyond, *Green Energy Environ.*, 2016, **1**, 18–42.
4 E. G. Yanes, S. R. Gratz, M. J. Baldwin, S. E. Robison and A. M. Stalcup, Capillary electrophoretic application of 1-alkyl-3-methylimidazolium-based ionic liquids, *Anal. Chem.*, 2001, **73**, 3838–3844.
5 A. Paul, S. Muthukumar and S. Prasad, Review-room-temperature ionic liquids for electrochemical application with special focus on gas sensors, *J. Electrochem. Soc.*, 2020, **167**, 037511.
6 C. Dai, J. Zhang, C. Huang and Z. Lei, Ionic liquids in selective oxidation: Catalysts and solvents, *Chem. Rev.*, 2017, **117**, 6929–6983.
7 S. Doherty, J. G. Knight, J. R. Ellison, P. Goodrich, L. Hall, C. Hardacre, M. J. Muldoon, S. Park, A. Ribeiro, C. A. N. de Castro, M. J. Lourenco and P. Davey, An efficient Cu(II)-bis(oxazoline)-based polymer immobilised ionic liquid phase catalyst for asymmetric carbon–carbon bond formation, *Green Chem.*, 2014, **16**, 1470–1479.
8 Z. Lei, B. Chen, Y.-M. Koo and D. R. MacFarlane, Introduction: Ionic liquids, *Chem. Rev.*, 2017, **117**(10), 6633–6635.
9 M. Galinski, A. Lewandowski and I. Stepniak, Ionic liquids as electrolytes, *Electrochim. Acta*, 2006, **51**, 5567–5580.
10 F. U. Shah, O. Gnezdilov and A. Filippov, Ion dynamics in halogen-free phosphonium bis(salicylato)borate ionic liquid electrolytes for lithium-ion batteries, *Phys. Chem. Chem. Phys.*, 2017, **19**, 16721–16730.
11 H. Rahman, H. Werth, A. Goldman, Y. Hida, C. Diesner, L. Lane and P. L. Menezes, Recent progress on electroactive polymers: Synthesis, properties and applications, *Ceramics*, 2021, **4**, 516–541.
12 J. Lee and T. Aida, ''Bucky gels'' for tailoring electroactive materials and devices: The composites of carbon materials with ionic liquids, *Chem. Commun.*, 2011, **47**, 6757–6762.
13 E. A. Muller, M. L. Strader, J. E. Johns, A. Yang, B. W. Caplins, A. J. Shearer, D. E. Suich and C. B. Harris, Femtosecond electron solvation at the ionic liquid/metal electrode interface, *J. Am. Chem. Soc.*, 2013, **135**, 10646–10653.
14 Y. Leng, J. Wang, D. Zhu, X. Ren, H. Ge and L. Shen, Heteropolyanion-based ionic liquids: Reaction-induced self-separation catalysts for esterification, *Angew. Chem.*, 2009, **121**, 174–177.
15 O. S. Morozov, S. S. Shachneva and A. V. Kepman, Microporous PVDF ionic membranes for actuator applications prepared with imidazole-based poly(ionic) liquid as a pore forming material, *Mater. Sci. Eng.*, 2019, **683**, 012060.
16 C. Dworak, S. C. Ligon, R. Tiefenthaller, J. J. Lagref, R. Frantz, Z. M. Cherkaoui and R. Liska, Imidazole-based ionic liquids for free radical photopolymerization, *Des. Monomers Polym.*, 2015, **18**, 262–270.
17 T. Wan, L. Zhou, K. Gong, K. Zhang, J. Zhang, X. Wang and Y. Yan, Molecular insights into the separation mechanism of imidazole-based ionic liquid supported membranes, *J. Mol. Liq.*, 2021, **340**, 117173.
18 P. Isosaari, V. Srivastava and M. Sillanpää, Ionic liquid-based water treatment technologies for organic pollutants: Current status and future prospects of ionic liquid mediated technologies, *Sci. Total Environ.*, 2019, **690**, 604–619.
19 A. A. Fannin, D. A. Floreani, L. A. King, J. S. Landers, B. J. Piersma, D. J. Stech, R. L. Vaughn, J. S. Wilkes and L. Williams John, Properties of 1,3-dialkylimidazolium chloride-aluminum chloride ionic liquids. 2. Phase transitions, densities, electrical conductivities, and viscosities, *J. Phys. Chem.*, 1984, **88**, 2614–2621.
20 M. D. Green and T. E. Long, Designing imidazole-based ionic liquids and ionic liquid monomers for emerging technologies, *Polym. Rev.*, 2009, **49**, 291–314.
21 Y. Tao, R. Dong, I. V. Pavlidis, B. Chen and T. Tan, Using imidazolium-based ionic liquids as dual solvent-catalysts for sustainable synthesis of vitamin esters: Inspiration from bio- and organo-catalysis, *Green Chem.*, 2016, **18**, 1240–1248.
22 M. Ghorbani and M. I. Simone, Developing new inexpensive room-temperature ionic liquids with high thermal stability and a greener synthetic profile, *ACS Omega*, 2020, **5**, 12637–12648.
23 A. E. Visser, R. P. Swatloski, W. M. Reichert, H. James, J. Davis, R. D. Rogers, R. Mayton, S. Sheff and A. Wierzbicki, Task-specific ionic liquids for the extraction of metal ions from aqueous solutions, *Chem. Commun.*, 2001, 135–136.
24 A. Visser, R. Swatloski, S. Griffin, D. Hartman and R. Rogers, Liquid/liquid extraction of metal ions in room temperature ionic liquids, *Sep. Sci. Technol.*, 2001, **36**, 785.
25 T. Ueki and M. Watanabe, Macromolecules in ionic liquids: Progress, challenges, and opportunities, *Macromolecules*, 2008, **41**, 3739–3749.
26 S. Lerch and T. Strassner, Expanding the electrochemical window: New tunable aryl alkyl ionic liquids (TAAILs) with dicyanamide anions, *Chem. – Eur. J.*, 2019, **25**, 16251–16256.
27 Q. Zhang, K. Liu, K. Liu, L. Zhou, C. Ma and Y. Du, Imidazole containing solid polymer electrolyte for lithium ion conduction and the effects of two lithium salts, *Electrochim. Acta*, 2020, **351**, 136342.
28 A. K. Gopalakrishnan, S. A. Angamaly and M. P. Velayudhan, An insight into the biological properties of imidazole-based Schiff bases: A review, *ChemistrySelect*, 2021, **6**, 10918–10947.
29 F. U. Shah, S. Glavatskih, P. M. Dean, D. R. MacFarlane, M. Forsyth and O. N. Antzutkin, Halogen-free chelated orthoborate ionic liquids and organic ionic plastic crystals, *J. Mater. Chem.*, 2012, **22**, 6928–6938.
30 J.-K. Kim, A. Matic, J.-H. Ahn and P. Jacobsson, An imidazolium based ionic liquid electrolyte for lithium batteries, *J. Power Sources*, 2010, **195**, 7639–7643.
31 J. Ding, W. B. Hu, E. Paek and D. Mitlin, Review of hybrid ion capacitors: From aqueous to lithium to sodium, *Chem. Rev.*, 2018, **118**, 6457–6498.
32 M. Li, J. Lu, Z. Chen and K. Amine, 30 Years of lithium-ion batteries, *Adv. Mater.*, 2018, **30**, 1800561.
33 P. Simon and Y. Gogotsi, Materials for electrochemical capacitors, *Nat. Mater.*, 2008, **7**, 845–854.
34 Y. Shao, M. F. El-Kady, J. Sun, Y. Li, Q. Zhang, M. Zhu, H. Wang, B. Dunn and R. B. Kaner, Design and mechanisms

of asymmetric supercapacitors, *Chem. Rev.*, 2018, **118**, 9233–9280.

35 J. A. Blazquez, J. Rodriguez, J. A. Pomposo and D. Mecerreyes, Tuning the solubility of polymerized ionic liquids by simple anion-exchange reactions, *J. Polym. Sci., Part A: Polym. Chem.*, 2004, **42**, 208–212.

36 K. Liu, W. Liu, Y. Qiu, B. Kong, Y. Sun, Z. Chen, D. Zhuo, D. Lin and Y. Cui, Electrospun core-shell microfber separator with thermaltriggered fame-retardant properties for lithium-ion batteries, *Sci. Adv.*, 2017, **3**, e1601978.

37 Y.-K. Sun, Z. Chen, H.-J. Noh, D.-J. Lee, H.-G. Jung, Y. Ren, S. Wang, C.-S. Yoon, S.-T. Myung and K. Amine, Nanostructured high-energy cathode materials for advanced lithium batteries, *Nat. Mater.*, 2012, **11**, 942.

38 M. Q. Xu, L. D. Xing, W. S. Li, X. X. Zuo, D. Shu and G. L. Li, Application of cyclohexyl benzene as electrolyte additive for overcharge protection of lithium ion battery, *J. Power Sources*, 2008, **184**, 427–431.

39 I. A. Khan, Y. L. Wang and F. U. Shah, Effect of structural variation in biomass-derived nonfluorinated ionic liquids electrolytes on the performance of supercapacitors, *J. Energy Chem.*, 2022, **69**, 174–184.

40 M.-T. F. Rodrigues, G. Babu, H. Gullapalli, K. Kalaga, F. N. Sayed, K. Kato, J. Joyner and P. M. Ajayan, A materials perspective on Li-ion batteries at extreme temperatures, *Nat. Energy*, 2017, **2**, 17108.

41 A. Guerfi, S. Duchesne, Y. Kobayashi, A. Vijh and K. Zagib, $LiFePO_4$ and graphite electrodes with ionic liquids based on bis(fluorosulfonyl)imide $(FSI)^-$ for Li-ion batteries, *J. Power Sources*, 2008, **175**, 866.

42 H. F. Xiang, Q. Y. Jin, C. H. Chen, X. W. Ge, S. Guo and J. H. Y. Sun, Dimethyl methylphosphonate-based nonflammable electrolyte and high safety lithium-ion batteries, *J. Power Sources*, 2007, **174**, 335.

43 K. Xu, M. S. Ding, S. S. Zhang, J. L. Allen and T. R. Jow, Evaluation of fluorinated alkyl phosphates as flame retardants in electrolytes for Li-ion batteries: I. Physical and electrochemical properties, *J. Electrochem. Soc.*, 2003, **150**, A161.

44 K. Xu, S. S. Zhang, J. L. Allen and T. R. Jow, Evaluation of fluorinated alkyl phosphates as flame retardants in electrolytes for li-ion batteries, *J. Electrochem. Soc.*, 2003, **150**, A170–A175.

45 F. Guo, Y. Ozaki, K. Nishimura, N. Hashimoto and O. Fujita, Experimental study on flame stability limits of lithium ion battery electrolyte solvents with organophosphorus compounds addition usinga candle-like wick combustion system, *Combust. Flame*, 2019, **207**, 63–70.

46 X. M. Wang, E. Yasukawa and S. Kasuya, Nonflammable trimethyl phosphate solvent-containing electrolytes for lithium-ion batteries: I. fundamental properties, *J. Electrochem. Soc.*, 2001, **148**, A1058.

47 Y. E. Hyung, D. R. Vissers and K. Amine, Flame-retardant additives for lithium-ion batteries, *J. Power Sources*, 2003, **119**, 383.

48 J. Arai, A novel non-flammable electrolyte containing methyl nonafluorobutyl ether for lithium secondary batteries, *J. Appl. Electrochem.*, 2002, **32**, 1071–1079.

49 J. Yamaki, I. Yamazaki, M. Egashira and S. Okada, Thermal studies of fluorinated ester as a novel candidate for electrolyte solvent of lithium metal anode rechargeable cells, *J. Power Sources*, 2001, **102**, 288.

50 K. Xu and C. A. Angell, Sulfone-based electrolytes for lithium-ion batteries, *J. Electrochem. Soc.*, 2002, **149**, A920.

51 Z. Zhao, D.-M. Guo, T. Fu, X.-L. Wang and Y.-Z. Wang, A highly-effective ionic liquid flame retardant towards fire-safety waterborne polyurethane (WPU) with excellent comprehensive performance, *Polymer*, 2020, **205**, 122780.

52 H. Nakagawa, Y. Fujino, S. Kozono, Y. Katatyama, T. Nukuda, H. Sakaebe, H. Matsumoto and K. Tatsumi, Application of nonflammable electrolyte with room temperature ionic liquids (RTILs) for lithium-ion cells, *J. Power Sources*, 2007, **174**, 1021.

53 X. Wu, K. Song, X. Zhang, N. Hu, L. Li, W. Li, L. Zhang and H. Zhang, Safety issues in lithium ion batteries: Materials and cell design, *Front. Energy Res.*, 2019, **7**, 65.

54 X. M. Zhu, X. Y. Jiang, X. P. Ai, H. X. Yang and Y. L. Cao, Bis(2,2,2-Trifluoroethyl) ethylphosphonate as novel high-efficient flame retardant additive for safer lithium-ion battery, *Electrochim. Acta*, 2015, **165**, 67–71.

55 J. Feng, P. Ma, H. Yang and L. Lu, Understanding the interactions of phosphonate-based flame-retarding additives with graphitic anode for lithium ion batteries, *Electrochim. Acta*, 2013, **114**, 688–692.

56 P. Shi, H. Zheng, X. Liang, Y. Sun, S. Cheng, C. Chen and H. Xiang, A highly concentrated phosphate-based electrolyte for high-safety rechargeable lithium batteries, *Chem. Commun.*, 2018, **54**, 4453–4456.

57 F. Wendler, L.-N. Todi and F. Meister, Thermostability of imidazolium ionic liquids as direct solvents for cellulose, *Thermochim. Acta*, 2012, **528**, 76–84.

58 A. W. T. King, A. Parviainen, P. Karhunen, J. Matikainen, L. K. J. Hauru, H. Sixta and I. Kilpelaïnen, Relative and inherent reactivities of imidazolium-based ionic liquids: The implications for lignocellulose processing applications, *RSC Adv.*, 2012, **2**, 8020–8026.

59 M. T. Clough, K. Geyer, P. A. Hunt, J. Mertes and T. Welton, Thermal decomposition of carboxylate ionic liquids: Trends and mechanisms, *Phys. Chem. Chem. Phys.*, 2013, **15**, 20480–20495.

60 R. Klein, O. Zech, E. Maurer, M. Kellermeier and W. Kunz, Oligoether carboxylates: Task-Specific room-temperature ionic liquids, *J. Phys. Chem. B*, 2011, **115**, 8961–8969.

61 I. A. Khan, O. I. Gnezdilov, A. Filippov and F. U. Shah, Ion transport and electrochemical properties of lithium-ion battery electrolytes derived from biomass, *ACS Sustainable Chem. Eng.*, 2021, **9**, 7769–7780.

62 F. U. Shah, O. I. Gnezdilov, I. A. Khan, A. Filippov, N. A. Slad and P. Johansson, Structural and ion dynamics in fluorine-free oligoether carboxylate ionic liquid-based electrolytes, *J. Phys. Chem. B*, 2020, **124**, 9690–9700.

63 F. Philippi, D. Rauber, B. Kuttich, T. Kraus, C. W. M. Kay, R. Hempelmann, P. A. Hunt and T. Welton, Ether functionalisation, ion conformation and the optimisation of macroscopic properties in ionic liquids, *Phys. Chem. Chem. Phys.*, 2020, **22**, 23038–23056.

64 I. A. Khan, O. I. Gnezdilov, Y. L. Wang, A. Filippov and F. U. Shah, Effect of aromaticity in anion on the cation-anion interactions and ionic mobility in fluorine-free ionic liquids, *J. Phys. Chem. B*, 2020, **124**, 11962–11973.

65 K. Hayamizu, S. Tsuzuki, S. Seki and Y. Umebayashi, Multinuclear NMR studies on translational and rotational motion for two ionic liquids composed of BF_4 anion, *J. Phys. Chem. B*, 2012, **116**, 11284–11291.

66 A. Filippov, A. S. Alexandrov, R. Gimatdinov and F. U. Shah, Unusual ion transport behaviour of ethylammonium nitrate mixed with lithium nitrate, *J. Mol. Liq.*, 2021, **340**, 116841.

67 A. Filippov, O. N. Antzutkin and F. U. Shah, Rapid carbene formation increasing ion diffusivity in an imidazolium acetate ionic liquid confined between polar glass plates, *Phys. Chem. Chem. Phys.*, 2019, **21**, 22531–22538.

68 C. Largeot, C. Portet, J. Chmiola, P.-L. Taberna, Y. Gogotsi and P. Simon, Relation between the ion size and pore size for an electric double-layer capacitor, *J. Am. Chem. Soc.*, 2008, **130**, 2730–2731.

69 I. A. Khan, A. Badshah, I. Khan, D. Zhao and M. A. Nadeem, Soft-template carbonization approach of MOF-5 to mesoporous carbon nanospheres as excellent electrode materials for supercapacitor, *Microporous Mesoporous Mater.*, 2017, **253**, 169–176.

70 I. A. Khan, M. Choucair, M. Imran, A. Badshah and M. A. Nadeem, Supercapacitive behavior of microporous carbon derived from zinc based metal–organic framework and furfuryl alcohol, *Int. J. Hydrogen Energy*, 2015, **40**, 13344–13356.

71 C. P. Fredlake, J. M. Crosthwaite, D. G. Hert, S. N. V. K. Aki and J. F. Brennecke, Thermophysical properties of imidazolium-based ionic liquids, *J. Chem. Eng. Data*, 2004, **49**, 954–964.

72 X. Mao, P. Brown, C. Červinka, G. Hazell, H. Li, Y. Ren, D. Chen, R. Atkin, J. Eastoe, I. Grillo, A. A. H. Padua, M. F. C. Gomes and T. A. Hatton, Self-assembled nanostructures in ionic liquids facilitate charge storage at electrified interfaces, *Nat. Mater.*, 2019, **18**, 1350–1357.

73 J. E. Tanner, Use of the stimulated echo in NMR diffusion studies, *J. Chem. Phys.*, 1970, **52**, 2523–2526.

